



ALEGRA: Finite element modeling for shock hydrodynamics and multiphysics

John H.J. Niederhaus^{*}, Steven W. Bova, James B. Carleton, John H. Carpenter, Kyle R. Cochrane, Michael M. Crockatt, Wen Dong, Timothy J. Fuller, Brian N. Granzow, Daniel A. Ibanez, Stephen R. Kennon, Christopher B. Luchini, Ramón J. Moral, Christopher J. O'Brien, Michael J. Powell, Allen C. Robinson, Angel E. Rodriguez, Jason J. Sanchez, W. Alan Scott, Christopher M. Siefert, Alan K. Stagg, Irina K. Tezaur, Thomas E. Voth, John R. Wilkes

Sandia National Laboratories, P.O. Box 5800, Albuquerque, 87185, NM, USA

ARTICLE INFO

Keywords:
Finite element
Multiphysics

ABSTRACT

ALEGRA is a multiphysics finite-element shock hydrodynamics code, under development at Sandia National Laboratories since 1990. Fully coupled multiphysics capabilities include transient magnetics, magnetohydrodynamics, electromechanics, and radiation transport. ALEGRA is used to study hypervelocity impact, pulsed power devices, and radiation effects. The breadth of physics represented in ALEGRA is outlined here, along with simulated results for a selected hypervelocity impact experiment.

1. Introduction

The ALEGRA code emerged from the experimental, theoretical, and computational shock wave research program that has been underway at Sandia National Laboratories since the 1950s [1]. That program cultivated the development of several technologies for modeling various aspects of shock hydrodynamics and solid mechanics on high-performance computing hardware. One of these technologies is the ALEGRA code, developed at Sandia since 1990 [2,3].

ALEGRA is designed to meet the need that had arisen among researchers and engineers for predictive modeling of shock wave phenomena, such as impact and blast, simultaneously with other physical mechanisms that drive or participate in the system behavior. These mechanisms include electrical circuits, electromagnetic fields and forces, resistive heating, piezo- and ferroelectric effects, thermal conduction, and radiative heat transfer. Those needs prompted the initial development of ALEGRA, which was strongly influenced by mature efforts in related areas [4–6]. These multiphysics needs continue to drive the development of the code.

The capabilities and reliability of ALEGRA have been discussed previously in Refs. [2,3]. In this paper, these capabilities are reviewed as they currently exist in the code, having advanced substantially over recent years.

The algorithms and features included in ALEGRA at present, as well as its limitations, are described below in Sections 2 and 4, and its modeling capabilities are demonstrated in Sections 3 and 5 by studying a laboratory example of hypervelocity impact. Some advanced features of ALEGRA are briefly outlined in Section 6.

2. Shock hydrodynamics capabilities

ALEGRA's core is an explicit solid dynamics algorithm based on arbitrary Lagrangian–Eulerian (ALE) technology, a concept originated by Hirt, Amsden, and Cook (1974) [7]. The implementation is intended to allow predictive modeling of large-deformation solid dynamics in two and three spatial dimensions, with an arbitrary number of materials that may co-exist within mixed-material elements. The primary components of this core are the solid dynamics algorithms that integrate the equations of motion and the material models that supply the closure properties in those equations.

^{*} Corresponding author.

E-mail address: jhniede@sandia.gov (J.H.J. Niederhaus).

2.1. Solid dynamics

ALEGRA (ALE General Research Application) uses a finite element discretization derived from the work of Taylor and Flanagan [4]. Four-node quadrilaterals are used in two dimensions (2D), and 8-node hexahedra in three dimensions (3D), with kinematic quantities (displacement, velocity, acceleration) centered on nodes and dynamic and thermodynamic quantities (stress, temperature, density) located on element centers. Nodal quantities are supported by linear shape functions, and element quantities are assumed to be uniform across the element. A uniform strain formulation with hourglass control is used to suppress zero-energy deformation modes while avoiding locking [8]. The Lagrangian equations of motion are solved using explicit time integration schemes. Detailed information on the accuracy, stability, and conservation properties of the midpoint predictor–corrector algorithm can be found in Refs. [9,10]. A legacy central difference method described in [11] is also available.

With this finite element kernel at its core, ALEGRA computes solutions to problems in solid dynamics by a three-step process on each time step: (1) compute Lagrangian motion using the linear finite element discretization and stresses from the previous time step, (2) evaluate material models to obtain stresses at the new time step, and (3) optionally, remap the solution fields to a stationary Eulerian mesh or to a smoothed mesh. In most current ALEGRA use cases, all three steps are used, but in some scenarios, ALEGRA can be used in Lagrangian mode, with contact algorithms to control the interaction between materials in the computational mesh. To accommodate the Lagrangian and ALE capabilities, ALEGRA uses an unstructured mesh representation. This allows body-fitted meshing when necessary, and also allows ALEGRA to support specialized non-orthogonal element shapes even for Eulerian models.

Since the propagation of shock waves on the discrete mesh is essential to modeling high-deformation solid dynamics, ALEGRA incorporates artificial viscosity methods to ensure that shocks can be captured without spurious oscillations. In ALEGRA's implementation, this is done by adding a viscous term to the stress during the Lagrangian step. This regularizes the equations which are otherwise inviscid, since surface tension and friction are omitted from the formulation. The artificial viscosity methods and their properties are described in detail in Refs. [3,12].

The most computationally expensive portion of the solid dynamics core of ALEGRA is the remap algorithm used for Eulerian and ALE simulations. The algorithm uses an operator-split “swept” scheme that can accommodate unstructured meshes. It handles staggered mesh variables (element versus node centering) using the half-interval shift method [13]. The remap algorithms in ALEGRA use upwinding, monotonic limiters, and higher-order reconstructions to ensure accuracy and stability of the Eulerian solution. The reconstruction is third-order-accurate in space in pure-material regions, but an adaptive scheme is used to adjust the reconstruction stencil for remapping based on the presence of mixed-material elements in the vicinity. This has been shown to improve the robustness of high-deformation solid dynamics simulations [14].

To accommodate multimaterial shock environments, mechanisms are in place to handle mixed-material elements, including both material interface reconstruction and multimaterial closure. ALEGRA does not allow diffusive molecular mixing or mixing layers. Materials are effectively considered to be immiscible, with a well-defined interface. Volume-of-fluid interface reconstruction methods are used to locate it on each timestep so that distinct materials will be remapped to neighboring elements in a less diffusive manner [15]. In elements that contain one or more material interfaces, a multimaterial closure must be used to compute mixture properties based on the thermodynamic state of each of the individual materials. The stresses used in the finite element kernel are the homogenized stresses. Advanced techniques

have been developed and implemented in ALEGRA to accomplish this homogenization with maximum accuracy and stability [14].

All of the algorithms in ALEGRA are enabled for parallel scalability using the Message Passing Interface (MPI) standard. This allows ALEGRA to be used extensively on traditional multicore supercomputer architectures, where solid dynamics simulations have demonstrated parallel scalability up to tens of thousands of cores [16]. Solid dynamics simulations with as many as 4 billion unknowns have been completed successfully.

2.2. Material models

After each Lagrangian step, and before remeshing/remapping, ALEGRA must update material states in order to obtain the stress tensor that will be used in the subsequent step. To support this, ALEGRA incorporates a broad range of material models simulating many different physics applications. The equation of state models include tabular equations of state such as SESAME [17] and LEOS [18], and analytical equations of state including Mie-Grüneisen, Vinet, and Jones–Wilkins–Lee (JWL). Tabular and parameterized analytic equation of state models for over 400 materials are available for use in ALEGRA, most of them encompassing solid, liquid, gas, and ionized plasma states. Also included are programmed burn and reactive burn models for explosives and reacting materials, as well as models for phase changes and non-equilibrium chemistry [19].

Hypo- and hyper-elastic constitutive models for various types of solids are included, covering metals, polymers, and brittle materials. Well-known metal strength models in ALEGRA include Johnson–Cook [20,21], Steinberg–Guinan–Lund [22], and others. Constitutive models for ceramic materials include the Kayenta model [23] and Johnson–Holmquist–Beissel [24], and stochastic microscale inhomogeneities inherent to these materials are represented using statistical variability incorporated natively into the initial conditions [25]. Most plasticity models are implemented in ALEGRA using an infinitesimal-strain approximation and a subset are available with finite-strain approximations [26]. ALEGRA also includes an interface for user-defined constitutive models, based on the “UMAT” and “VUMAT” conventions [27], which are compiled at run time.

For multiphysics simulations, ALEGRA carries tabular and analytical models for electrical conductivity, thermal conductivity, magnetization, ionization, and opacity. The majority of these models have been vetted against experimental data obtained from platforms such as gas guns or Sandia's Z machine, as well as calculations based on density functional theory or molecular dynamics. Examples can be found in Refs. [28–30].

2.3. Limitations

There are several important limitations of ALEGRA's solid dynamics capabilities. First, although ALEGRA has advanced ALE capabilities, they are not generally used in terminal ballistics or pulsed power modeling. The ALE technology in ALEGRA has proven very useful in certain situations [31,32]. However, most of the applications of ALEGRA appearing in the literature for various classes of problems [33–35] have used purely Eulerian meshes, including those shown here in Sections 3 and 5. This is because remesh and mesh smoothing is problematic for conformal representation of the opening and closure of gaps between materials in terminal ballistics, and there are ambiguities associated with selecting smoothing techniques and target element shapes for scenarios with high strain rates and strong shear.

Second, ALEGRA simulations are costly to execute. This is due to the stability limitation on the explicit time step, as well as the infrastructure required to support unstructured meshes, remesh/remap, and multiphysics couplings. Robustness issues can compound the cost and difficulty of these simulations, as faulty conditions including negative element volume and imaginary sound speeds can arise in the course of solid dynamics simulations.

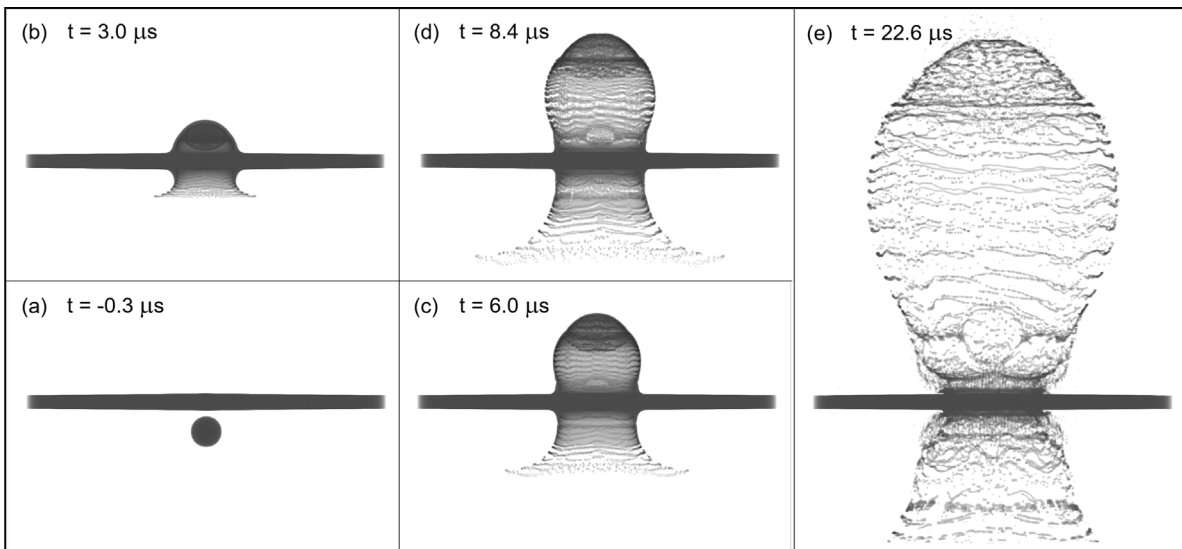


Fig. 1. Radiographic projection of material density from ALEGRA results for the aluminum-sphere impact experiments of Piekutowski [36] at 6.68 km/s.

Third, certain physical phenomena and capabilities are not included. There is no possibility of modeling structural mechanics implicitly, which means that structural dynamics, vibration, and fluid-structure interactions cannot easily be captured. Also excluded are any notion of physical fluid viscosity, surface tension, and diffusive or molecular mixing. The restriction to 4-node quadrilateral and 8-node hexahedral elements also imposes practical limitations when meshes conformal to material interfaces may be desirable.

Finally, the capabilities are limited by the physical fidelity and consistency of the constitutive relationships and material data that supply closures for the equations being integrated. The predictive realism of simulations in ALEGRA across a wide range of thermodynamic states relies on the accuracy of the empirical and theoretical material science providing relevant non-linear material properties [1].

3. Hypervelocity impact example

With these capabilities and limitations in mind, here we evaluate the ALEGRA code for modeling hypervelocity impact, using one of the gas gun tests published by Piekutowski in 1993 [36]. Those tests characterized the debris cloud emerging behind an aluminum plate due to normal impact of an aluminum sphere at speeds between 3 and 8 km/s, for purposes of studying damage due to meteoroid impact in spacecraft. Piekutowski's study included many well-resolved x-radiograph images of the impact event, along with tabulated spatial measurements of the evolving debris cloud. Both of these lend themselves well to validation of codes like ALEGRA, particularly for the well-known aluminum alloys used in the laboratory shots.

For brevity, only one of those tests is simulated here using ALEGRA: the case with a sphere diameter of 9.53 mm, an impact velocity of 6.68 km/s, and a plate thickness of 4.039 mm. This test is referred to as shot 4-1353. Radiographs at $t = 8.4$ and $22.6 \mu\text{s}$ after impact appear in the final panel of Figure 3 in Ref. [36]. Image times and other details of the experiments are found in Ref. [37].

Shot 4-1353 is modeled here in ALEGRA on a uniform 3D Eulerian mesh with 380 million elements and a resolution of 0.15 mm (27 elements across the plate thickness). Material models for the aluminum alloys used in the test include the Mie-Grüneisen equation of state model and the Steinberg-Guinan-Lund yield model, with appropriate tensile stress limits (damage) and a probabilistic perturbation of the initial yield stress using a Weibull distribution (11% variance) sampled randomly for each material. The simulation runs for 7 h on 3840 processors (2.9 GHz Intel Cascade Lake), with a timestep of approximately

4 ns, producing the results shown in Fig. 1. Here, volume rendered-images are generated using radiographic projection in ParaView [38], with the material density as the opacity variable.

The simulation results shown in Fig. 1(d,e) can be compared to experimental images in Figure 3 of Ref. [36]. The simulations demonstrate the same phenomenology described by Piekutowski, including the trumpet-shaped ejecta veil recoiling from the impact side of the plate, and the bulbous debris bubble emerging from the rear of the plate. As observed by Piekutowski for this thickest plate from his test set, all that remains of the projectile is a cloud of very fine, presumably liquid droplets near the head of the bubble.

These features can be seen side-by-side in Fig. 2, where the simulation results at $t = 8.4, 22.6 \mu\text{s}$ are shown again, alongside the corresponding experimental radiograph for shot 4-1353. The radiograph is reproduced from Figure 3 in Ref. [36], with permission from the publisher. Spatial measurements of the debris cloud length for shot 4-1353 can be found in Table 3 of Piekutowski's technical report in Ref. [37]. In that report, the axial length of the debris bubble at $t = 22.6 \mu\text{s}$ is listed as $4.36 \pm 0.01 \text{ in} = 11.07 \pm 0.03 \text{ cm}$. The ALEGRA simulation finds a debris bubble length of $4.425 \pm 0.006 \text{ in} = 11.24 \pm 0.02 \text{ cm}$. This exceeds the measured value by only 1.5%.

Since no spatial scale appears with the experimental radiographs in Refs. [36] or [37], a scale based on the debris bubble length itself is applied instead. Using the above values of the debris bubble length at $t = 22.6 \mu\text{s}$, the experimental and numerical images at $t = 8.4, 22.6 \mu\text{s}$ are each scaled spatially to reproduce the 1.5% difference. These scaled images are juxtaposed in Fig. 2.

It should be noted that the radiographic projection used here in ParaView relies on attenuation along collimated sampling paths, while the experimental radiographs used a series of non-collimated sources. (See Figure 3 in Ref. [37].) Although the measured values were corrected for parallax, the radiographs were not. Therefore, there is parallax in the radiographs that is not captured in the numerical results, which we believe accounts for visible differences in the apparent thickness of the plate. It should also be noted that certain details of the simulation results are known to be influenced by mesh resolution, statistical perturbation of the initial condition, and numerical artifacts. These include the banded structure of the debris bubble, the fine structure of the ejecta veil, and the size of individual fragments.

The experimental procedure for shot 4-1353 did not produce any measured transverse dimensions of the debris bubble, or a measured bubble length for $t = 8.4 \mu\text{s}$. Nevertheless, the direct comparison provided in Fig. 2 demonstrates qualitatively that the transverse and axial

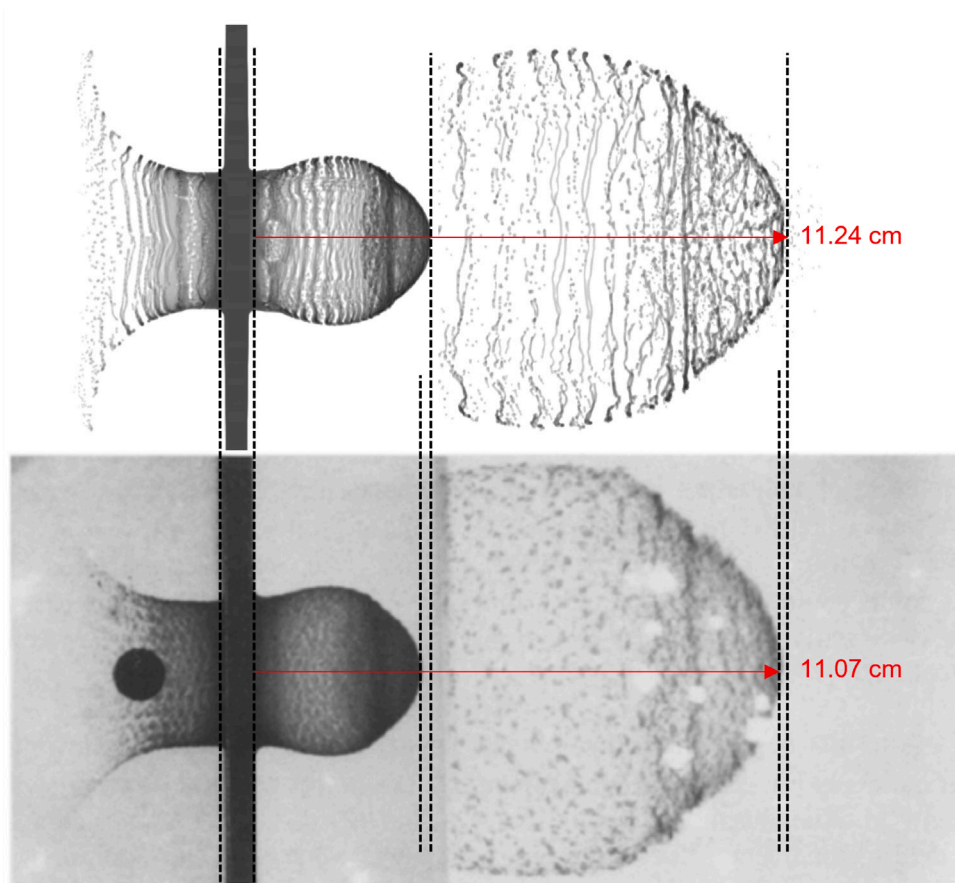


Fig. 2. Comparison of computational (top) and experimental (bottom) radiographs for the aluminum-sphere impact experiments of Piekutowski [36] at 6.68 km/s. Experimental radiograph is reprinted with permission.

dimensions of the laboratory debris bubble are captured by ALEGRA, both at the earlier and later X-ray flash times. Reference lines have been added to the images to aid in comparison.

In Ref. [36], Piekutowski used the analysis of Anderson (1990) [39] to infer that the projectile material may be liquefied during impact at this velocity. The ALEGRA simulation confirms this, finding that most of the projectile material has exceeded the melt temperature used in the yield model. The simulation provides a reliable model for macroscopic features of the system, consistent with previous validation studies for ALEGRA in hypervelocity impact and terminal ballistics [2,40–42].

4. Multiphysics capabilities

Although solid dynamics modeling forms the foundation for ALEGRA, much additional value is obtained by adding multiphysics capabilities. The capabilities include several forms of magnetohydrodynamics (MHD), electromechanics, diffusive thermal transport, and radiation transport using a diffusion equation approximation as well as implicit Monte Carlo (IMC) and deterministic methods. A steady state electric potential solve is required for electromechanical modeling as well as the MHD variants.

These multiphysics capabilities are generally included through first-order-in-time operator splitting algorithms so that the various force contributions and diffusive effects are tightly coupled while running at the stability limit associated with the hydrodynamic time step. The diffusion transport operators are implemented implicitly in order to avoid stability concerns arising from the potential for stiff diffusive operators.

4.1. Solvers

ALEGRA requires scalable multi-level solvers that aim to solve linear systems in approximately $O(N)$ operations for N degrees of freedom. To achieve scalable performance for elliptic problems and stiff diffusive operators, multilevel algebraic multigrid solvers are utilized. ALEGRA's implicit multi-level solvers traditionally use the Trilinos open source library software [43]. Recently, however, due to the importance of discovering and utilizing the best scalable solver technologies, the Hypr software library [44] has also been made available as an option for use in magnetohydrodynamic modeling.

Current ALEGRA users may now require problem sizes greater than 2 billion unknowns. It is thus necessary to upgrade the internal meshing infrastructure and the next generation of solvers that allow for integer identifiers with more than 32 bits using C++ templating. Transitioning from the Trilinos Epetra to the newer Tpetra interface is in progress to support very large scale computations. ALEGRA utilizes a number of external software libraries and Trilinos and Hypr are prime examples. Managing and upgrading these packages directly from the corresponding source is now accomplished using the Spack package manager [45].

4.2. Magnetohydrodynamics

There are two major production-level MHD modeling capabilities in ALEGRA. The most common model is “resistive MHD.” This model keeps Faraday’s law but neglects displacement currents in Ampère’s Law. When these two equations are combined with Ohm’s law which relates the current density in Ampère’s Law to the co-moving electric

field, one obtains a parabolic magnetic diffusion or transport equation. The Maxwell divergence-free law for the magnetic flux density is enforced discretely as an involution just as in the continuous Maxwell equations [3].

To ensure a proper discrete diffusion operator and ease of application of boundary condition in 3D, the electric field is represented using edge elements and the flux density using face elements. The electric field can be represented as a sum of a steady state potential equation and a diffusive response equation which allows for the application of potential boundary conditions. Electric and magnetic field-based tangential boundary conditions are also supported. The magnetic diffusion equation requires a specialized H(curl) solver to deal with the large null space of the discrete curl-curl stiffness matrix. For magnetic flux density in the plane the 2D algorithm is a nodal representation and is essentially a projection of the 3D algorithm to 2D. For historical reasons, a scalar magnetic field out of the plane is represented with a nodal discretization and thus this implementation is distinctly different [46].

The resistive MHD algorithm contains an ideal MHD step with an explicit time step based on the fastest ideal magnetosonic wave speed, a constrained transport remap that ensures that the discrete zero divergence of the flux density is maintained, followed by an operator split magnetic diffusion that provides the Joule heating [47]. Since the fast magnetosonic wave speed is unbounded as the density goes to zero a force limiter option may be necessary for problems that generate low density material [48].

A second but much simpler model is the so-called low-magnetic-Reynolds-number or “low- R_m ” case which assumes that magnetic diffusion is so fast relative to other time scales of interest that the $\mathbf{J} \times \mathbf{B}$ forces can be neglected relative to the effects of the Joule energy deposition [49]. For shock physics time scales, this simplification becomes sensible primarily for physically very small systems with an associated large Ohmic energy deposition. The low- R_m approximation results in an elliptic form of the equation governing magnetic transport, eliminating the need for a specialized H(curl) solver. As a result, the low- R_m MHD capability provides a substantial reduction in computational cost compared to resistive MHD. Both of these MHD capabilities can be coupled to external lumped element circuit models to properly account for coupled energy entering and/or leaving the simulated domain depending on the simulation dynamics.

Current research focuses on removing inconsistencies found in the resistive MHD model near low-density regions. These include questions of how to retain displacement currents in the model [50], and how to effectively include Hall terms in an Extended MHD model that involves a current density equation with a stiff source term associated with the plasma frequency, while still running at useful engineering hydrodynamic times scales.

4.3. Electromechanics

ALEGRA also combines the shock physics infrastructure with the quasi-static electric (QSE) field approximation of Maxwell’s equations [51] and is complementary to the magneto-quasi-static (MQS) approximation used in MHD. The QSE approximation is valid for time scales of interest that are much longer than the speed of light transit time scales. All dielectrics are considered perfectly nonconducting, and all conductors assumed to be perfectly conducting and are modeled as constant potential bodies or surfaces. The free charge density in dielectrics is assumed to be zero. An operator split solution methodology [52] is employed to solve the coupled electromechanical equations. The Sundials differential algebraic equation (DAE) package [53] allows coupling of ALEGRA with a user-defined circuit.

Several electromechanical material models are available that describe dielectric, piezoelectric, and ferroelectric (FE) materials. The “linear dielectric fluid” model implements a simple linear relationship between electric displacement and electric field and is used with a

mechanical EOS to compute the stress, adding electric-field-dependent terms. The “piezoelectricity” model is a general implementation of the linear piezoelectric equations of state [54]. The constitutive equations are expressed in the stress-charge form and no material symmetry assumptions are made. In the “nonlinear piezoelectricity” model, the electromechanical coefficient tensors may be specified as functions of the stress and electric field components.

The “fe afe ceramic” model provides the electromechanical response of an FE material that, under sufficient mechanical load, transforms to an antiferroelectric (AFE) phase and undergoes both a large change in polarization and a significant inelastic strain as a result. Current development focuses on improvements to ferroelectric models. This includes improvements to the “fe afe ceramic” model to account for effects of transformation under anisotropic stress as well as a general model for ferroelectrics, based on a micromechanical approach with energy-based switching criteria that captures both domain reorientation and phase transformation phenomena. The general ferroelectric model is accompanied by a corresponding surrogate model tailored for simulating domain reorientation and FE to AFE phase transformation.

4.4. High-energy-density physics

The “high-energy density physics” (HEDP) capabilities in ALEGRA include all of the MHD capabilities mentioned in Section 4.2, along with radiative heat transport and opacity models for absorption and scattering of radiation. The HEDP capabilities are useful for modeling systems that involve plasmas or plasma generation and/or gain or lose a significant fraction of energy via radiation. For example, these may include systems for laser- or X-ray-driven ablation, pulsed power, or spark discharges.

There are three radiation transport capabilities in ALEGRA. For cases with isotropic radiation geometry and optically thick media (small photon mean free path), multigroup diffusion is available. This solves a diffusion approximation to the Boltzmann equation for a series of photon energy groups, using iterative Trilinos solvers and energy-dependent opacity models. For cases where the radiation geometry is anisotropic (e.g., for beams and collimated sources) and/or the medium may be optically thick or thin, a fully-integrated IMC capability is available, based on the Kull IMC package [55], and a deterministic capability is available via coupling with the SCEPTRE package [56]. All three radiation transport options can be used with the solid/hydrodynamics capabilities in ALEGRA to model radiation-hydrodynamics, and the multigroup diffusion model can be used for radiation MHD, including thermal conduction as well. The HEDP features in ALEGRA been used successfully for scientific applications found in Refs. [3,57, 58].

4.5. Multiphysics limitations

The multiphysics capabilities in ALEGRA are also subject to several significant limitations. Most importantly, nearly all of them rely on at least one iterative solver that must satisfy a convergence criterion on every cycle of the calculation. Particularly for the case of 3D resistive MHD, as mentioned in Section 4.2, the magnetic diffusion equation being solved has a large near null space that requires advanced multilevel preconditioners. Even with the advanced Trilinos and HyPre solvers implemented in ALEGRA, analysts are sometimes forced either to use a relatively loose convergence criterion, or accept very large solve times, resulting in a costly simulation with a long turnaround time. Options are available in ALEGRA for overcoming some of the consequences of this difficulty, and research has helped to establish optimal solver configurations [59].

The scope of physics included in ALEGRA’s multiphysics modules is also limited. Although MHD and electromechanics are supported, many important aspects of electromagnetism are excluded, such as dielectric breakdown and multi-fluid or kinetic aspects of plasmas. However, the operator-splitting algorithms implemented in ALEGRA do admit the possibility of adding other physics modules.

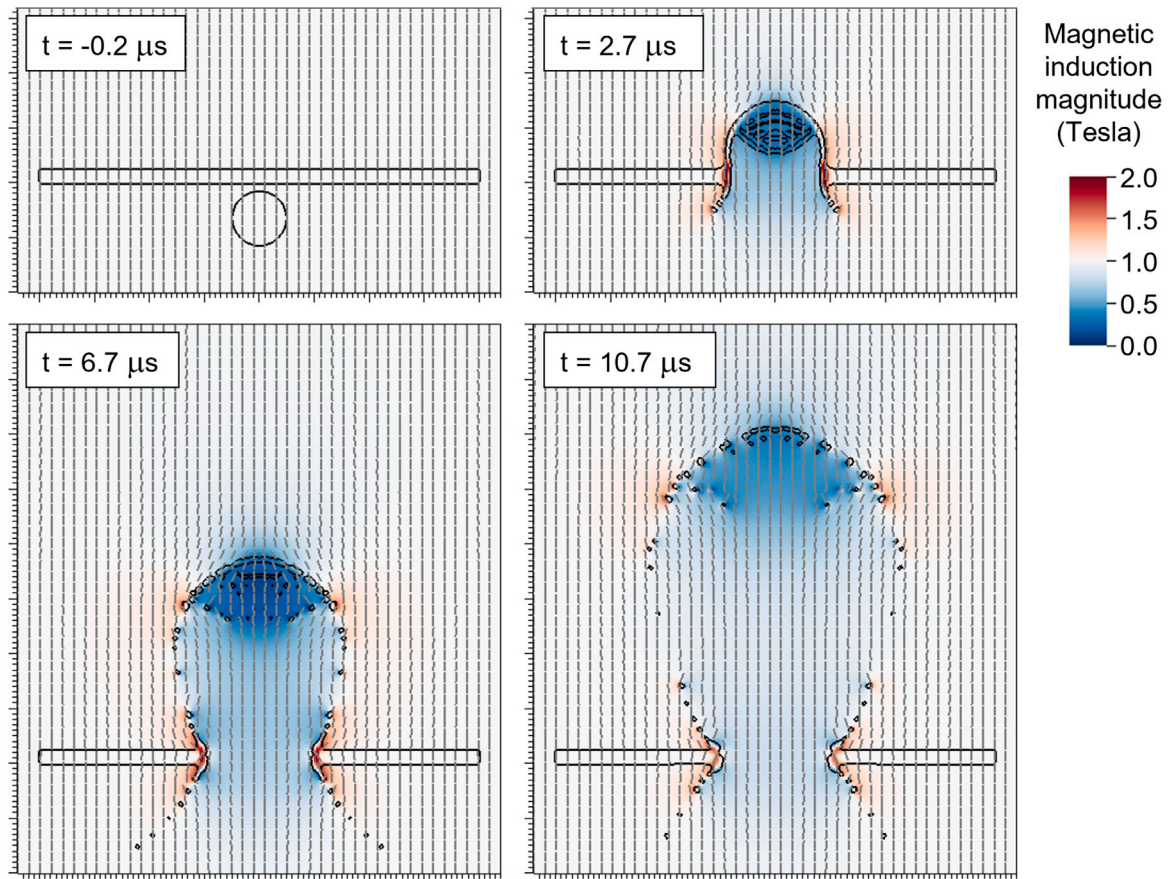


Fig. 3. Slice view of the magnetic induction magnitude during impact at 6.68 km/s in an initially uniform axial magnetic field of 1 T. Glyphs are overlaid indicating the local orientation of the magnetic induction.

5. Magnetized hypervelocity impact examples

To evaluate one portion of the multiphysics capabilities of ALEGRA, two contrived examples are considered here. Both involve the resistive MHD capability, with electromagnetic fields involved in hypervelocity impact.

In the first scenario, the setup of experimental shot 4–1353 of Piekutowski [36] is notionally extended to include a preexisting uniform 1-Tesla magnetic field. The magnetic field is aligned with the projectile flight path in the z -direction, and it permeates the entire domain at time zero, including the interior of the projectile sphere. Lee–More–Desjarlais electrical conductivity models [28] are assigned to the materials, and the Trilinos multi-level transient magnetic diffusion solver is enabled. The simulation uses constrained transport remap on a uniform Eulerian mesh with a resolution of 0.3 mm (13 elements across the plate thickness). Imposing quarter symmetry reduces the mesh to 12 million elements. The mesh is twice as coarse as that used for the original hypervelocity impact simulation in Section 3, due to the additional computational cost associated with resistive MHD. The simulation runs to 10 μ s in 10 h on 288 processors (2.1 GHz Intel Broadwell), with a timestep generally remaining near 8 ns.

In this scenario, since all motion is along the z -direction prior to impact, the magnetic field does not change and there is no electric current until impact. At impact, transverse velocities appear in the projectile and target. Since these materials are electrical conductors, this generates eddy currents and distorts the magnetic field, deflecting it and sweeping it radially out of the impact zone.

The ALEGRA model captures this behavior, as seen in the simulation results in Fig. 3, which show a slice view of the 3D domain during the

impact event at $y = 0$. Black contours of the material volume fraction demonstrate the progress of the debris bubble formation, similar to that seen in Section 3. A blue-to-red color mapping indicates the magnitude of the magnetic flux density vector field (also known as magnetic induction or B field), while gray glyphs indicate the orientation of the field. For spatial reference, the distance between large tick marks in these plots is 1 cm. The field magnitude increases visibly immediately outside of the impact zone and debris bubble, while a region of suppressed or near-zero magnetic field develops in the impact zone and the debris bubble interior, where the motion of the conducting material has swept away the magnetic field. The motion of the conducting metal fragments also visibly deflects the field in the vicinity of the debris bubble. The suppression of the B field in the bubble interior persists until the debris bubble breaks up later in time.

In the second scenario, shot 4–1353 of Piekutowski [36] is extended differently, in this case by making the projectile sphere a permanent magnet. The sphere is magnetized in the $+z$ -direction, but no external magnetic field is imposed in this scenario. Additionally, four conducting coils and an associated electric circuit are added to the setup such that the passage of the sphere and debris cloud can be detected via electromagnetic induction. Inductive coils have been used successfully in this way for experiments in impact physics in many previous studies [60–62]. Numerical simulations of electromagnetic induction during impact have also been demonstrated successfully, but in English-language journals they are generally limited to scenarios without any large deformations [60,61,63].

In the ALEGRA simulations for this scenario, notional single-turn copper coils are present in the Eulerian impact model and connected to ALEGRA's lumped element circuit model via internal boundary

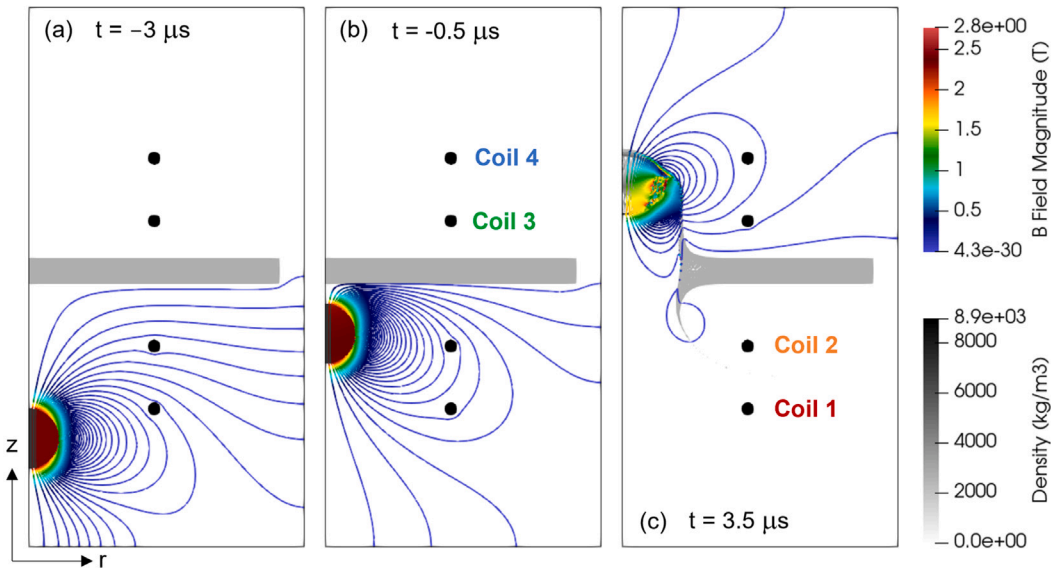


Fig. 4. Magnetic field lines associated with impact of a neodymium-alloy sphere magnet at 6.68 km/s, encircled by four induction coils.

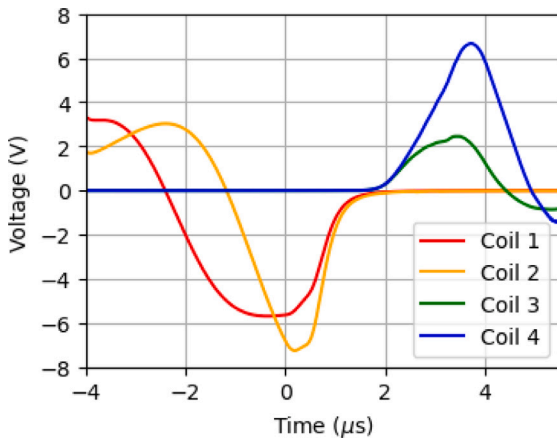


Fig. 5. Voltage pulses generated on inductive coils during the simulated impact shown in Fig. 4.

conditions, each in series with a 1-Ω resistor. This allows the electromotive force (emf) generated in the coils to be captured. The coils are numbered 1 through 4, in the order in which the projectile and debris bubble will pass through them and generate a voltage signal. The coils have a diameter of 40 mm, and they are inserted both upstream and downstream from the target plate. To minimize the computational cost and allow for a finer mesh, these simulations are conducted using 2D axisymmetry. The mesh is a uniform Eulerian grid in the $r - z$ plane with a resolution of 50 μm and 1.5 million elements. The magnetic field is assumed to lie everywhere within the plane, and the electric field and currents are everywhere normal to the plane in the circumferential direction, but Joule heating is omitted. The sphere has approximately the magnetization and mechanical properties of an N42-grade neodymium-alloy magnet. Its magnetization is assumed to be permanent, even though in reality it would vanish due to the shock environment during impact.

The magnetic field of the sphere and its interaction with these coils during approach and impact on the aluminum plate at 6.68 km/s are shown in Fig. 4. Magnetic field lines are shown overlaid on a grayscale plot of the material density, colored by the magnitude of the magnetic induction vector, B , in Tesla. The conducting target plate

initially confines most the magnetic field to the upstream region, until the impact event ruptures the plate, allowing the field to emerge at the rear.

As the magnetic field passes through the coils, it induces an emf on the order of a few volts, and a current on the order of a few Amperes flows normal to the plane (circumferentially) and through the connected resistor to counteract the change in enclosed magnetic flux. Fig. 5 shows the voltage signals in the four coils as captured by ALEGRA’s circuit model. Each of the pulses forms a bipolar waveform similar to the signals seen in sensor coils in Refs. [60–62], The signal on the coil has positive voltage during the approach of the sphere, switching to negative voltage when the sphere exits each coil. The presence of the plate and the compression and fragmentation of the magnetic material by the impact event both disrupt the signal, but the simulation successfully captures the coupling of electromagnetic induction with impact physics.

These example scenarios demonstrate the utility of the ALEGRA resistive MHD capability in both 2D and 3D for capturing eddy currents, electromagnetic induction, and magnetic diffusion in fully coupled fashion with high-deformation solid dynamics. Previous work has similarly demonstrated the other multiphysics capabilities in ALEGRA, for electromechanical effects [64] and radiation hydrodynamics [34,58].

6. Advanced capabilities

Several advanced features of ALEGRA provide further utility and versatility. First, an implementation of the eXtended Finite Element Method (XFEM) [65] has been devised for and incorporated into ALEGRA as a means of handling material interfaces in Eulerian solid dynamics as internal element discontinuities while retaining the convergence properties of the base finite element discretization [66,67]. The method provides multiple kinematic fields per multi-material element, and defines surfaces across which the materials can interact via contact, allowing sliding and gap opening and closure to occur within an Eulerian framework. The capability is fully enabled for 2D solid dynamics, and for 3D, work is underway to replace the traditional “swept” remap algorithm with an intersection-based scheme.

Second, ALEGRA also provides the ability to generate parametric, optimization, and uncertainty quantification studies in automated fashion from within ALEGRA input using the DAKOTA package [68]. Parameterized inputs are passed directly from DAKOTA to ALEGRA, and response function information is passed directly back to DAKOTA.

Entire sets of ALEGRA simulations can be run within a DAKOTA framework, in a single instance of ALEGRA. Tools for introducing aleatory uncertainty into an ALEGRA model are also available, for example by applying mathematically defined statistical distributions to material model parameters across the domain.

Third, the ability to couple multiple instances of ALEGRA, or one instance of ALEGRA with an instance of some other software, is supported by the code. Currently, ALEGRA MHD and electromechanical simulations can be coupled to one another via a common circuit model, and ALEGRA can be coupled to radiation-transport software for purposes of radiation-hydrodynamics modeling. This is accomplished using the MPI multiple-program-multiple-data (MPMD) launch mode.

Lastly, ALEGRA's shock-multiphysics capabilities are being enabled for "next-generation" accelerator-based architectures such as GPUs. Currently, the focus of this work is on Cartesian-grid Eulerian multi-material hydrodynamics and low-magnetic-Reynolds-number MHD. Some modernizations are being applied as this is done, including the move to an unsplit intersection-based remap scheme and the use of second-order predictor–corrector time integration by default. Achieving any reduction in time-to-solution for simulations using the current ALEGRA code on traditional architectures will be difficult, given the size of the code base and the extent of optimization that has already been done. This transition to support for "next-generation" hardware will provide a critical alternative route for future engineers to achieve the modeling throughput that they will need.

7. Conclusions

The ALEGRA software includes a very broad array of mature numerical modeling capabilities for high-deformation solid dynamics coupled to electromagnetics and radiation. It has demonstrated reliability in physics-based modeling of impact physics and terminal ballistics, and its usefulness in multiphysics modeling of pulsed-power and radiation energy deposition systems is also well established. Validation studies like those shown here and listed in the References have strengthened this foundation. Looking to the future, it is anticipated that development efforts will continue to deepen the physical fidelity of ALEGRA simulations, and expand the scope of computing architectures where ALEGRA and its capabilities can be used with the desired modeling throughput. This will provide future researchers with tools to advance the understanding of multiphysics-coupled high-deformation solid dynamics systems.

CRedit authorship contribution statement

John H.J. Niederhaus: Originated the manuscript, Wrote portions of the text, Conducted physics analysis using the ALEGRA software, Created figures, Accumulated references. **Steven W. Bova:** Code development/manuscript review. **James B. Carleton:** Helped draft and edit electromechanics section of text, Code development, Software testing, Verification, Validation, Material model development. **John H. Carpenter:** Material model, Code development. **Kyle R. Cochran:** Material model development. **Michael M. Crockatt:** Code development. **Wen Dong:** Material model development, Verification, Validation. **Timothy J. Fuller:** Code development, Material model development, Software infrastructure. **Brian N. Granzow:** Code development. **Daniel A. Ibanez:** Code development. **Stephen R. Kennon:** Code development. **Christopher B. Luchini:** Code development. **Ramón J. Moral:** Software testing, Physics analysis. **Christopher J. O'Brien:** Verification, Validation, Material model development. **Michael J. Powell:** ALEGRA developer. Helped draft and edit the manuscript. **Allen C. Robinson:** Code development, Writing – review & editing. **Angel E. Rodriguez:** Software testing, Physics analysis. **Jason J. Sanchez:** Code development, Material model development. **W. Alan Scott:** Scientific visualization supporting synthetic radiographs. **Christopher M. Siefert:** Developer of ALEGRA code used in the paper. **Alan K. Stagg:**

laser energy deposition code development. **Irina K. Tezaur:** Code development, Paper revisions. **Thomas E. Voth:** Originator of several algorithms (XFEM, REMESH) described in manuscript, Reviewed manuscript and made edits. **John R. Wilkes:** Executed simulations, Supported code-development efforts.

Declaration of competing interest

The authors declare that they have no known competing financial interests or personal relationships that could have appeared to influence the work reported in this paper.

Data availability

The data will be made available on request. The software can be released with appropriate authorization.

Acknowledgments

Special thanks to Bill Rider of Sandia for technical review of this manuscript. This work was sponsored in part by the U.S. Army. Sandia National Laboratories is a multimission laboratory managed and operated by National Technology and Engineering Solutions of Sandia, LLC., a wholly owned subsidiary of Honeywell International, Inc., for the U.S. Department of Energy's National Nuclear Security Administration under contract DE-NA0003525.

References

- [1] Asay JR, Chhabildas LC, Lawrence RJ, Sweeney MA. Impactful times: Memories of 60 years of shock wave research at sandia national laboratories. New York: Springer-Verlag; 2017. <http://dx.doi.org/10.1007/978-3-319-33347-2>.
- [2] Summers RM, Peery JS, Wong MK, Jr. ESH, Trucano TG, Chhabildas LC. Recent progress in ALEGRA development and application to ballistic impacts. Int J Impact Eng 1997;20:779–88. [http://dx.doi.org/10.1016/S0734-743X\(97\)87463-5](http://dx.doi.org/10.1016/S0734-743X(97)87463-5).
- [3] Robinson AC, et al. ALEGRA: An arbitrary Lagrangian-Eulerian multimaterial, multiphysics code. In: Proceedings of the 46th AIAA aerospace sciences meeting, AIAA-2008-1235. 2008. <http://dx.doi.org/10.2514/6.2008-1235>.
- [4] Taylor LM, Flanagan DP. PRONTO 3D : A three-dimensional transient solid dynamics program. Technical report SAND87-1912, Albuquerque, NM: Sandia National Laboratories; 1989. <http://dx.doi.org/10.2172/6212624>.
- [5] McGlaun J, Thompson S, Elrick M. CTH: A three-dimensional shock wave physics code. Int J Impact Eng 1990;10(1):351–60. [http://dx.doi.org/10.1016/0734-743X\(90\)90071-3](http://dx.doi.org/10.1016/0734-743X(90)90071-3).
- [6] Tipton R. CALE users manual. Technical report, Livermore, CA: Lawrence Livermore National Laboratories; 1995.
- [7] Hirt CW, Amsden AA, Cook JL. An arbitrary Lagrangian-Eulerian computing method for all flow speeds. J Comput Phys 1974;14(3):227–53. [http://dx.doi.org/10.1016/0021-9991\(74\)90051-5](http://dx.doi.org/10.1016/0021-9991(74)90051-5).
- [8] Flanagan DP, Belytschko T. A uniform strain hexahedron and quadrilateral with orthogonal hourglass control. Int J Numer Methods Eng 1981;17:679–706. <http://dx.doi.org/10.1002/nme.1620170504>.
- [9] Love E, Rider WJ, Scovazzi G. Stability analysis of a predictor/multi-corrector method for staggered-grid Lagrangian shock hydrodynamics. J Comput Phys 2009;228(20):7543–64. <http://dx.doi.org/10.1016/j.jcp.2009.06.042>.
- [10] Love E, Scovazzi G, Rider W. Algorithmic properties of the midpoint predictor-corrector time integrator. Technical report, SAND2009-1127, New Mexico: Sandia National Laboratories; 2009.
- [11] Love E, Wong M. Lagrangian continuum dynamics in ALEGRA. Tech. rep. SAND2007-8104, Albuquerque, NM: Sandia National Laboratories; 2007. <http://dx.doi.org/10.2172/934850>.
- [12] Rider WJ, Love E, Scovazzi G, Weirs VG. A high resolution Lagrangian method using nonlinear hybridization and hyperviscosity. Comput & Fluids 2013;83:25–32. <http://dx.doi.org/10.1016/j.compfluid.2012.09.009>.
- [13] Peery JS, Carroll DE. Multi-material ALE methods in unstructured grids. Comput Methods Appl Math 2000;187:591–619. [http://dx.doi.org/10.1016/S0045-7825\(99\)00341-2](http://dx.doi.org/10.1016/S0045-7825(99)00341-2).
- [14] Rider WJ, Love E, Wong MK, Strack OE, Petney SV, Labreche DA. Adaptive methods for multi-material ALE hydrodynamics. Int J Numer Methods Fluids 2011;65:1325–37. <http://dx.doi.org/10.1002/fld.2365>.
- [15] Mosso SJ, Garasi CJ, Drake RR. A smoothed two- and three-dimensional interface reconstruction method. Comput Vis Sci 2009;12:365–81. <http://dx.doi.org/10.1002/fld.2365>.

- [16] Niederhaus JHJ, Drake RR, Luchini CB. Parallel scaling analysis for explicit solid dynamics in ALEGRA. Technical report SAND2015-11038, Albuquerque, NM: Sandia National Laboratories; 2015, <http://dx.doi.org/10.2172/1957761>.
- [17] Lyon SP, Johnson JD. SESAME: The LANL equation of state database. Technical report LA-UR-92-3407, Los Alamos, NM: Los Alamos National Laboratory; 1992.
- [18] Gaffney JA, Hu SX, Arnault P, et al. A review of equation-of-state models for inertial confinement fusion materials. High Energy Dens Phys 2018;28:7–24. <http://dx.doi.org/10.1016/j.hedp.2018.08.001>.
- [19] Moore N, Sanchez J, Hobbs M, Lane J, Long K. Model for photothermal ionization and molecular recombination during pulsed ablation of polyethylene. J Appl Phys 2020;128:125902. <http://dx.doi.org/10.1063/5.0017566>.
- [20] Johnson G, Cook W. A constitutive model and data for metals subjected to large strains, high strain rates, and high temperatures. In: Proc. 7th int. symposium on ballistics. 1983, p. 541.
- [21] Sanchez JJ. The finite strain johnson cook plasticity and damage constitutive model in ALEGRA. Technical report SAND2018-1392, Albuquerque, NM: Sandia National Laboratories; 2018, <http://dx.doi.org/10.2172/1423181>.
- [22] Steinberg DJ, Cochran SG, Guinan MW. A constitutive model for metals applicable at high-strain rate. J Appl Phys 1980;51(3):1498–504. <http://dx.doi.org/10.1063/1.327799>.
- [23] Brannon RM, Fuller TJ, Strack OE, Fossom AF, Sanchez JJ. KAYENTA: Theory and users' guide. Technical report SAND2015-0803, Albuquerque, NM: Sandia National Laboratories; 2015, <http://dx.doi.org/10.2172/1238100>.
- [24] Johnson G, Holmquist T, Beissel S. Response of aluminum nitride (including a phase change) to large strains, high strain rates and high pressures. J Appl Phys 2003;94(3):1639–46. <http://dx.doi.org/10.1063/1.1589177>.
- [25] Strack OE, Leavy RB, Brannon RM. Aleatory uncertainty and scale effects in computational damage models for failure and fragmentation. Internat J Numer Methods Eng 2015;102(3–4):468–95. <http://dx.doi.org/10.1002/nme.4699>.
- [26] Sanchez J. Inelastic equation of state for solids. Comput Methods Appl Mech Eng 2021;375. <http://dx.doi.org/10.1016/j.cma.2020.113622>.
- [27] ABAQUS user's manual. Providence, Rhode Island, USA: Dassault Systemes Simula Corp.; 2013, Version 6.13.
- [28] Desjarlais MP, Kress JD, Collins LA. Electrical conductivity for warm, dense aluminum plasmas and liquids. Phys Rev E 2002;66:025401. <http://dx.doi.org/10.1103/PhysRevE.66.025401>.
- [29] Porwitzky A, Cochrane KR, Stoltzfus B. Determining the electrical conductivity of metals using the 2 MA Thor pulsed power driver. Rev Sci Instrum 2021;92:053551. <http://dx.doi.org/10.1063/5.0037870>.
- [30] Cochrane KR, Kalita P, Brown JL, McCoy CA, Gluth JW, Hanshaw HL, Scoglietti E, Knudson MD, Rudin SP, Crockett SD. Platinum equation of state to greater than two terapascals: Experimental data and analytical models. Phys Rev B 2022;105:224109. <http://dx.doi.org/10.1103/PhysRevB.105.224109>.
- [31] Voth TE, Bishop JE. Semi-infinite target penetration by ogive-nose penetrators: ALEGRA/SHISM code predictions for ideal and non-ideal impacts. J Press Vessel Technol 2009;131(1):011205. <http://dx.doi.org/10.1115/1.3013859>, 1639–1646.
- [32] Niederhaus JHJ, Yang P, Diantonio C, Vunni G. Finite-element modeling for an explosively loaded ferroelectric generator. Technical report SAND2019-12669, Albuquerque, NM: Sandia National Laboratories; 2019, <http://dx.doi.org/10.2172/1571553>.
- [33] Carroll DE, Jr. ESH, Trucano TG. Simulation of armor penetration by tungsten rods: ALEGRA validation report. Technical report SAND97-2765, Albuquerque, NM: Sandia National Laboratories; 1997, <http://dx.doi.org/10.2172/560859>.
- [34] Lemke RW, Knudson MD, Bliss DE, Cochrane K, Davis J-P, Giunta AA, Harjes HC, Slutz SA. Magnetically accelerated, ultrahigh velocity flyer plates for shock wave experiments. J Appl Phys 2005;98:073530. <http://dx.doi.org/10.1063/1.2084316>.
- [35] Neal W, Garasi C. High fidelity studies of foil initiator bridges, part 3: ALEGRA-MHD simulations. AIP Conf Proc 2017;1793(080008). <http://dx.doi.org/10.1063/1.4971614>.
- [36] Piekutowski AJ. Characteristics of debris clouds produced by hypervelocity impact of aluminum spheres with thin aluminum plates. Int J Impact Eng 1993;14:573–86. [http://dx.doi.org/10.1016/0734-743X\(93\)90053-A](http://dx.doi.org/10.1016/0734-743X(93)90053-A).
- [37] Piekutowski AJ. Formation and description of debris clouds produced by hypervelocity impact. Technical report NASA CR-4707, NASA Marshall Space Flight Center; 1995, <https://hadlandimaging.com/wp-content/uploads/2021/06/NASA-CR4707-Report-1996.pdf>, accessed April, 2023.
- [38] ParaView. 2022, <https://paraview.org>, accessed July, 2022.
- [39] Anderson CE, Trucano TJ, Mullin SA. Debris cloud dynamics. Int J Impact Eng 1990;9:89–113. [http://dx.doi.org/10.1016/0734-743X\(90\)90024-P](http://dx.doi.org/10.1016/0734-743X(90)90024-P).
- [40] Zellner MB, Vunni GB. Photon Doppler velocimetry (PDV) characterization of shaped charge jet formation. Proc Eng 2013;58:88–97. <http://dx.doi.org/10.1016/j.proeng.2013.05.012>.
- [41] Portone T, Niederhaus J, Sanchez J, Swiler L. Bayesian model selection for metal yield models in high-velocity impact. Int J Impact Eng 2020;137:103459. <http://dx.doi.org/10.1016/j.ijimpeng.2019.103459>.
- [42] Doney RL, Niederhaus JHJ, Fuller TJ, Coppinger MJ. Effects of equations of state and constitutive models on simulating copper shaped charge jets in ALEGRA. Int J Impact Eng 2020;136:103428. <http://dx.doi.org/10.1016/j.ijimpeng.2019.103428>.
- [43] The trilinos project website. 2022, <https://trilinos.github.io>, accessed July, 2022.
- [44] Hypre: High Performance Preconditioners, <https://lnl.gov/casc/hypre>, <https://github.com/hypre-space/hypre>.
- [45] Spack: A Flexible Package Manager for HPC software, <https://computing.lnl.gov/projects/spack-hpc-package-manager>, <https://spack.readthedocs.io/>.
- [46] Ashcraft CC, Niederhaus JH, Robinson AC. Verification and validation of a coordinate-transformation method in axisymmetric transient magnetics. Technical report SAND2016-0804, Albuquerque, NM: Sandia National Laboratories; 2016, <http://dx.doi.org/10.2172/1237004>.
- [47] Robinson AC, et al. Arbitrary Lagrangian-Eulerian 3D ideal MHD algorithms. Int J Numer Methods Fluids 2011;65(11–12):1438–50. <http://dx.doi.org/10.1002/fld.2395>.
- [48] Robinson AC. On the utility of the Boris approach for dealing with fast magnetosonic wave speeds in an ALE MHD modeling context. Technical report SAND2011-4962C, Albuquerque, NM: Sandia National Laboratories; 2011.
- [49] Zwick D, Ibanez-Granados D. Simulation of Low-Rm physics in complex geometries on GPUs with LGR. Technical report SAND2021-11359, Albuquerque, NM: Sandia National Laboratories; 2021, <http://dx.doi.org/10.2172/1820251>.
- [50] McGregor D, Robinson A. An indirect ALE discretization of single fluid plasma without a fast magnetosonic time step restriction. Comput Math Appl 2019;78(2):417–36. <http://dx.doi.org/10.1016/j.camwa.2018.10.012>, Proceedings of the Eighth International Conference on Numerical Methods for Multi-Material Fluid Flows (MULTIMAT 2017).
- [51] Melcher JR. Continuum electromechanics. Cambridge, Massachusetts: MIT Press; 1981, Available at <http://ocw.mit.edu>.
- [52] Fish J, Chen W. Modeling and simulation of piezocomposites. Comput Methods Appl Mech Eng. 2003;192:3211–32. [http://dx.doi.org/10.1016/S0045-7825\(03\)00343-8](http://dx.doi.org/10.1016/S0045-7825(03)00343-8).
- [53] Hindmarsh AC, Brown PN, Grant KE, Lee SL, Serban R, Shumaker DE, Woodward CS. SUNDIALS: Suite of nonlinear and differential/algebraic equation solvers. ACM Trans Math Software 2005;31(3):363–96. <http://dx.doi.org/10.1145/1089014.1089020>.
- [54] Haskins J, Hickman J. A derivation and tabulation of the piezoelectric equations of state. J Acoust Soc Am 1950;22:584–8. <http://dx.doi.org/10.1121/1.1906655>.
- [55] Brunner TA, Urbatsch TJ, Evans TM, Gentile NA. Comparison of four parallel algorithms for domain decomposed implicit Monte Carlo. J Comput Phys 2006;212(2):527–39. <http://dx.doi.org/10.1016/j.jcp.2005.07.009>.
- [56] Bruss DE, Drumm CR, Fan WC, Pautz SD. SCEPTRE 2.2 quick start guide. Technical report SAND2021-3073, Albuquerque, NM: Sandia National Laboratories; 2021, <http://dx.doi.org/10.2172/1773011>.
- [57] Lemke RW, Sinars DB, Waisman EM, Cuneo ME, Yu EP, Hail TA, Hanshaw HL, Brunner TA, Jennings CA, Stygar WA, Desjarlais MP, Mehlhorn TA, Porter JL. Effects of mass ablation on the scaling of X-Ray power with current in wire-array Z-pinch. Phys Rev Lett 2009;102:025005. <http://dx.doi.org/10.1103/PhysRevLett.102.025005>.
- [58] Moore NW, Sanchez JJ, Schaeuble M-A, Hinshelwood D, Harvey-Thompson A, Myers CE, Jones B, Franke BC. Validation of ablation model for polyethylene using pulsed x-ray and proton exposures. J Appl Phys 2022;132(23):235901. <http://dx.doi.org/10.1063/5.0130799>.
- [59] Doney R, Siefert C, Niederhaus J. Improved solver settings for 3D exploding wire simulations in ALEGRA. Technical report ARL-TR-7748, Aberdeen Proving Ground, MD: US Army Research Laboratory; 2016, <http://dx.doi.org/10.2172/1562202>.
- [60] Uhlig WC, Heine A. Electromagnetic diagnostic techniques for hypervelocity projectile detection, velocity measurement, and size characterization: Theoretical concept and first experimental test. J Appl Phys 2015;118:184901. <http://dx.doi.org/10.1063/1.4935086>.
- [61] Wu X, Akram MS, Liu F-S, Xu Q-Y, Yang K, Li W-Q, Li JJ, Ma X-J. Simulation based study of magnetic velocity induction system by using Analysis System Electromagnetics Suite. Rev Sci Instrum 2021;92(9):094708. <http://dx.doi.org/10.1063/5.0050383>.
- [62] Adachi T, Miyara K, Ishii Y. Non-contact measurement of impact load due to collision of ferromagnetic projectile based on electromagnetic induction. Int J Impact Eng 2022;159:104040. <http://dx.doi.org/10.1016/j.ijimpeng.2021.104040>.
- [63] Zhang XL, Qi SP, Zhang Z, Wu C, Liu CA. Multi-physics finite element simulation of electromagnetic induction velocimetry under ultra-high-speed loading. Sci Technol Inf (Chinese) 2017;3:1. <http://dx.doi.org/10.16661/j.cnki.1672-3791.2017.32.001>.
- [64] Drumm MC. Computational simulation of explosively generated pulsed power devices. (Master's thesis), US Air Force Institute of Technology; 2013, <https://scholar.afit.edu/etd/826/>.
- [65] Moës N, Dolbow J, Belytschko T. A finite element method for crack growth without remeshing. Int J Numer Methods Eng 1999;46(1):131–50. [http://dx.doi.org/10.1002/\(SICI\)1097-0207\(199909\)46:1<131::AID-NME726>3.0.CO;2-J](http://dx.doi.org/10.1002/(SICI)1097-0207(199909)46:1<131::AID-NME726>3.0.CO;2-J).
- [66] Voth T, Mosso S. An extended finite element/Eulerian (XFEM/Eulerian) approach for solid mechanics. 2012, ARL Research in Ballistic Protection Technologies Workshop (presentation), <https://www.osti.gov/servlets/purl/1294175>.
- [67] Voth T, Niederhaus J, Mosso SJ, Luchini C, Kramer R. XFEM for 2- and 3-D multi-material Eulerian hydrodynamics in ALEGRA. 2017, MultiMat 2017 (poster), <https://www.osti.gov/servlets/purl/1470915>.
- [68] DAKOTA. 2022, <https://dakota.sandia.gov>, accessed July, 2022.